https://doi.org/10.5194/egusphere-2025-3036
Preprint. Discussion started: 7 July 2025


# Numerical simulation of magma-rock interaction at Krafla volcano using OpenFOAM software and a simplified thermal model

Muriel Gerbault[1], Oleg Melnik[2], and Anastassia Borisova[1]

[1]GET (IRD, CNRS, CNES, UPS, OMP), 14 av. E. Belin, Toulouse 31400, France
[2]Earth Science Department, University of Oxford, UK

**Correspondence:** Oleg Melnik (oleg.melnik@earth.ox.ac.uk)

**Abstract.** We present a 2D numerical modelling study aimed at exploring magma-rock interaction following the emplacement of a magmatic sill into cold shallow crust. An interface-tracking solver was developed, based on the open-source OpenFOAM package that enables simulation of heat and momentum transfer between magmas of different compositions, with contrasting densities, thermal properties, temperatures, crystal contents, and strain-rate dependent viscosities. Two scenarios are considered to reconstruct sharp temperature gradients and explain the presence of fresh rhyolitic fragments excavated from approximately 2 km depth during IDDP-1 drilling at Krafla caldera in 2009: partial melting of felsic crust triggered by either (1) a 300 m thick rhyolite intrusion or (2) a 100 m thick basalt sill. We also assume two possible magma emplacement periods: during the Krafla Fires (1975–1984, ∼35 years before drilling) and the Myvatn Fires (1724–1729, ∼300 years before drilling). In scenario (1), vigorously convective molten rhyolite produces a temperature jump (400°C) over approximately 25 meters (∼16°C/m) 35 years after emplacement. After 300 years, the thickness of these molten rocks reaches approximately 75 m, however, the thermal gradient becomes too small (less than 5 °C/m) to explain the IDDP-1 observations. In scenario (2), because of large density contrasts between the injected basaltic magma and molten rhyolite, two separate convective layers are formed. The thickness of molten rocks exceeds 30 m after 30 years. The rapid melting front propagation causes a sharp temperature gradient in the undisturbed rocks (28°C/m). We conclude that the second scenario provides a more reliable explanation for the existing data and is well supported by previous petrological studies. By comparing with a simplified 1D thermal model and performing parametric tests, we argue that our numerical approach is suitable for studying magmatic convection at such extremely high Rayleigh and Prandtl numbers.

## 1 Introduction

In several volcanic areas around the world, magma bodies were accidentally penetrated by drilling with the aim of discovering deep supercritical hydrothermal resources (e.g. Teplow et al., 2008). One of the first wells was drilled in the Krafla geothermal field in 2008–2009 by the Iceland Deep Drilling Project (IDDP-1). The well was designed to reach supercritical conditions at 4500 m depth, but at ∼2000 m depth, drilling became difficult due to a sharp increase in temperature. Finally, drilling stopped at 2096 m depth, and cuttings of fresh rhyolitic glass indicated the presence of a magma body at the bottom.

https://doi.org/10.5194/egusphere-2025-3036
Preprint. Discussion started: 7 July 2025


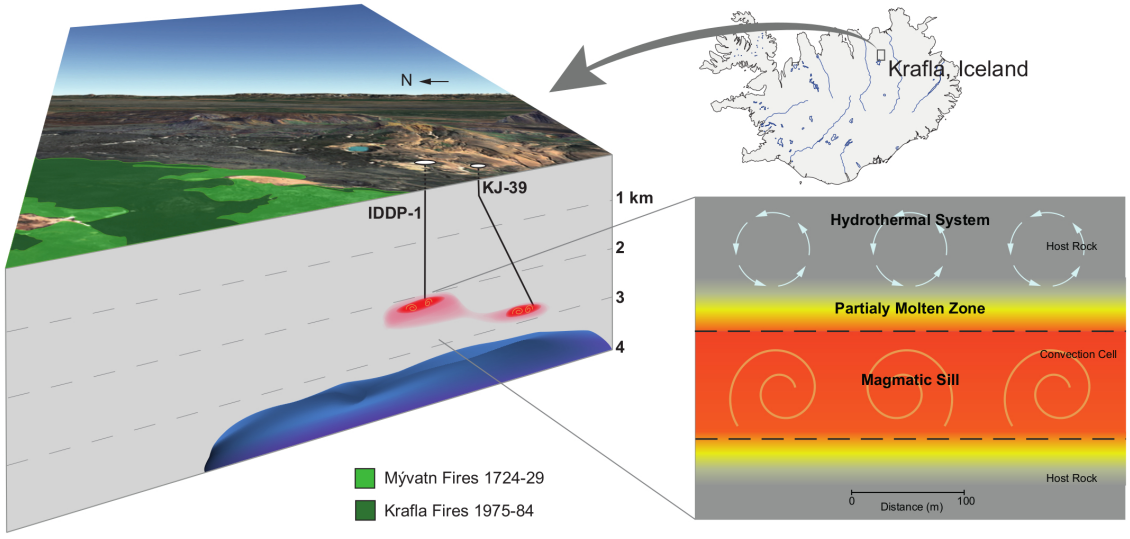


**Figure 1.** Conceptual setting of Krafla, Iceland: right, a 3D view displays IDDP-1 and KJ-39 drilling sites approaching a magma body at ca. 2 km depth (red), over geophysical anomalies located at depths greater than 3 km (purple). Left: this magma body is composed of partially molten host felsic rock above a (convecting) magmatic sill intrusion. We will not consider the overlying hydrothermal system here.

In the Menengai caldera in Kenya, geothermal drilling began in 2011, and since then multiple wells have penetrated syenitic magma 2 km below the caldera floor (Mbia et al., 2014). Not only were these magma bodies surprisingly shallow, but none of these magmas have erupted in recent times. At both the Krafla and Menengai sites, there was an abrupt transition from solid rock to molten magma with an extreme temperature gradient, as predicted by Carrigan (1984).

Krafla, one of the five volcanic systems in Iceland's North Volcanic Zone, recently recorded two major eruptive events: the Myvatn Fires in 1724–1729, and the Krafla Fires in 1975–1984 (e.g. Hollingsworth et al., 2012). While the 2009 IDDP-1 drilling showed magma at 2 km depth, seismic wave attenuation indicated a magma storage zone at rather 3 to 7 km depth (Schuler et al., 2015; Einarsson, 1978; Kim et al., 2020), coinciding with the geodetic-modelled depth to an inflating/deflating body during the Krafla Fires (Tryggvason, 1984), Fig. 1 (purple domain). The spatial extent and dimensions of this magma body at 2 km depth remain poorly constrained, as well as its composition, whether basaltic or felsic. But whatever its composition, the presence of a sharp temperature gradient as witnessed by the IDDP-1 drilling indicates convective heat transfer, because otherwise, conductive heat transfer would have rapidly smoothed it over time. According to Eichelberger (2020), the temperature increased from 500 to 900°C within only 25 meters during the IDDP-1 drilling. Such a high temperature gradient (>16°C/m) requires active melting of the crust.

According to drilling logs (Mortensen et al., 2014), the crust above the magma body in Krafla has a felsic composition. The magma uplifted by the drilling fluid also has a high silica content and ranges from crystal-free rhyolites to partially molten felsites or granophyres (Borisova et al., 2023). The debate about the nature of the intruding magma body is long-standing (e.g. Zierenberg et al., 2013; Rooyakkers et al., 2021), and whether not only basaltic but also rhyolitic magma intrusions caused

https://doi.org/10.5194/egusphere-2025-3036
Preprint. Discussion started: 7 July 2025


the production of the felsic magma drilled in the KJ-39 and IDDP-1 wells between 2008 and 2009 (Mortensen et al., 2010). Bimodal compositions of the erupted products were noticed since Grönvold and Mäkipää (1978), with lavas north of the caldera being more primitive than those inside the caldera during the first three eruptions (1975–1977). Until today, petrological studies indicate that a single reservoir cannot explain this bimodality (e.g. Rooyakkers et al., 2021). The recent study of Rooyakkers et al. (2024) invokes the necessity of short basalt–rhyolite mixing timescales (e.g., hours or days) and the ascent of both primitive and evolved basaltic magmas, driven by episodes of plate-boundary rifting during the Krafla Fires.

Available experimental studies of Icelandic rhyolite crystallization and felsite partial melting demonstrated the efficiency of partial melting of felsite crust (Masotta et al., 2018), while a numerical model of assimilation (Simakin and Bindeman, 2022) established the kinetics of convective dissolution due to compositional convection (where the reaction is controlled by convective transport). Masotta et al. (2018) suggested that the IDDP-1 rhyolite magma was formed by high-degree partial melting of a quartzo-feldspathic rock (granophyre) at shallow depth. Subsequently, the hot silicic magma generated may have intruded a second felsite (granophyre) lens located at a shallower crustal level, inducing low degrees of partial melting of the crystalline rock, corresponding to the process advocated by Simakin and Bindeman (2022). Based on analyses of the IDDP-1 zircons, Borisova et al. (2023) considered the viability of this scenario but suggested that the intrusion of basalt into the shallow felsic crust followed by its melting is a more plausible scenario to produce the magma extracted during the IDDP-1 drilling. These authors proposed that a magmatic sill of basaltic composition in its superheated state (at temperature above the magma liquidus temperature) intruded into and interacted directly with the predominantly felsic crust during the Krafla Fires. With the help of a one-dimensional (1D) thermochemical model, Borisova et al. (2023) explored the parametric range for a basaltic sill to produce the observed high temperature gradients $\sim$35 years after the intrusion. As a follow-up numerical study, the present contribution aims to compare the two propositions of a felsic or a basalt intrusion triggering convective heat transfer in overlying crust, with the support of two-dimensional (2D) and 1D thermo-mechanical models. We present below the physical and numerical assumptions, then the results and their limitations. Our results help improve our understanding of such magmatic dynamics and feed constraints for further drilling projects (e.g. Eichelberger et al., 2020).

## 2 Physical formulation and numerical setting

The problem of basaltic magma-felsic rock interaction was studied both experimentally and analytically by several authors (Huppert and Sparks, 1988; Carrigan, 1984). A review of different aspects of this problem can be found in a special collection "Magma-Rock and Magma-Mush Interactions as Fundamental Processes of Magmatic Differentiation" published in Frontiers (Borisova et al., 2021). Vigorous convection in a magma body intruded into cold host rock can induce advective heat transfer and melting of the overlying rocks. In these studies, magma intrusion is assumed instantaneous and its temperature is assumed to remain constant due to intense convective mixing. A thermal boundary layer (TBL) forms due to rapid cooling of the magma at the interface with the cold host rocks (Fig 2, between depths $D$ and $D + a$).

If the hot intruded magma is rhyolitic and identical to the host rocks, a single convective cell develops and its upper boundary progressively propagates upwards (the melting front). This layer of molten host rock maintains a uniform temperature, while

https://doi.org/10.5194/egusphere-2025-3036
Preprint. Discussion started: 7 July 2025


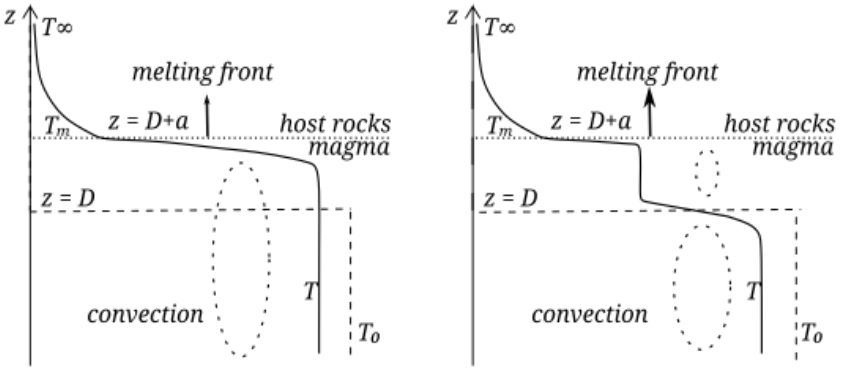


**Figure 2.** Sketch of geometry and mean temperature profiles, modified after (Huppert and Sparks, 1988): $T_o, T_{inf}, T_m$ are initial hot, top, and melt temperatures respectively, $D$ the intrusion thickness and $a$ the molten host rock layer thickness. a) Case of rhyolite intrusion similar to the host rock (scenario 1), b) Case of basaltic intrusion into rhyolitic host rock (scenario 2).

heat transfer remains conductive above it. If the melting front propagation rate is faster than the conductive timescale, a sharp temperature gradient develops across the molten/unmolten boundary (Fig 2, left at depth $D + a$). After some time, the whole system cools down and convection shuts down, leading to the retraction of the melting front and the return to a conductive heat profile.

In the case of a basaltic magma intrusion, the density contrast between the intruded magma and the molten host rock remains high, preventing intense mixing, and a two-layer convection structure forms as shown in Fig. 2.

### 2.1 System of equations

In order to model the physical setting presented above, we consider a numerical approach that solves the Navier-Stokes equations for incompressible fluids, with temperature- and crystal content-dependent viscosities, able to account for both compositional and thermal convection and for the release of latent heat of crystallization. The physical problem is described with the following equations of conservation of momentum, temperature and continuity:

$$\rho\frac{\partial \mathbf{U}}{\partial t} + \rho\mathbf{U}\cdot\nabla\,\mathbf{U} = -\nabla P + \rho\mathbf{g} + \nabla\cdot[\mu(\nabla\mathbf{U} + (\nabla\mathbf{U})^T)], \tag{1}$$

$$\rho C_p\left[\frac{\partial T}{\partial t} + \mathbf{U}\cdot\nabla T\right] = \nabla\cdot(\kappa\nabla T), \tag{2}$$

$$\nabla\cdot\mathbf{U} = 0. \tag{3}$$

https://doi.org/10.5194/egusphere-2025-3036
Preprint. Discussion started: 7 July 2025


$U$ stands for the velocity field, $P$ for pressure, $T$ for temperature, $g$ for gravity, $\rho$ and $\mu$ are density and dynamic viscosity. Thermal conductivity $\kappa$ and heat capacity $C_p$ vary with temperature. Further details are provided in section 2.2.

We adapted the *multiMeltInterFoamv2* solver (Louis-Napoleon et al., 2020, 2022; Louis-Napoléon et al., 2024) based on the VOF (Volume of Fluid) method implemented in the open-source platform OpenFOAM; this method was shown to track well the evolution of distinct immiscible fluid phases and, therefore, solves an additional conservation equation for material interfaces $C_i$ (here $i = 1$ for rhyolite and $i = 2$ for basalt material "phases"):

$$\frac{\partial C_i}{\partial t} + \mathbf{U} \cdot \nabla C_i = -\nabla \cdot (\mathbf{U}_r C_r), \tag{4}$$

The $-\nabla \cdot (\mathbf{U}_r C_r)$ term aims at reducing the effects of numerical smearing of phase interfaces, with $C_r = C_1.(1 - C_1)$ and $U_r$ a 'compression velocity', evaluated as a volume flux based on the maximum velocity magnitude in the interface region (Berberović et al., 2009). See Louis-Napoleon et al. (2022) for details and method validation.

### 2.2 Mechanical and thermal properties

We assume that density does not depend on pressure but depends on temperature (the Boussinesq approximation) and on melt fraction M, with reference densities for the solidus and liquidus states of each phase (see Table1 for values):

$$\rho = \rho_{ref} \times [1 - \alpha(T - T_{ref})], \text{ with } \rho_{ref} = \sum_{i=1}^{3} C_i \times [\rho_i^{S0}(1 - M) + \rho_i^{L0} M]. \tag{5}$$

Melt fraction $M$ is parametrized for each phase $i$ as:

$$\begin{aligned} &M = (1 + a_i + b_i T_r + c_i T_r^2 + d_i T_r^3)^{-1}. \\ &T_r = T/T_{ref_i}, T_{ref} = 1000^o C, \end{aligned} \tag{6}$$

with parameters obtained by fitting simulation results of the crystallization of basaltic and rhyolitic magmas with typical Krafla composition (Borisova et al., 2023), using the MELTS software (Gualda et al., 2012).

The thermal conductivity $\kappa$ and heat capacity $C_p$ are prescribed as:

$$C_p = C_{p_0} + L_* \frac{dM}{dT}, \kappa = \frac{\kappa_0}{1 + \kappa_T T}, \tag{7}$$

with $L_*$ the latent heat of crystallization, $\kappa_0$ and $\kappa_T$ constants given in Table 1.

Dynamic viscosity $\mu = \mu_m(T)\eta(\phi, \epsilon)$ is a product of melt viscosity $\mu_m$ given by Giordano et al. (2008) and a relative viscosity $\eta$ due to the presence of crystals, that depends on the melt fraction $M$ and the strain rate $\epsilon$ according to Costa et al. (2009):

$$\begin{aligned} &\log \mu_m = A_i + \tfrac{E_i}{T - C_i}, \\ &\eta(\phi, \epsilon) = \tfrac{1 + \phi^\delta}{[1 - F(\varphi, \epsilon, \gamma)]^{B\phi_*}} \\ &F = (1 - \xi) \cdot \text{erf}\left[\tfrac{\sqrt{\pi}}{2 \cdot (1 - \xi)} \varphi \cdot (1 + \varphi^\gamma)\right] \quad \text{with } \varphi = \tfrac{\phi}{\phi_*}, \phi = 1 - M. \end{aligned} \tag{8}$$

Constants $A_i, E_i, C_i$ differ between rhyolite and basalt phases ($i$), parameters $\delta, \phi_*, B, \xi, \gamma$ are strain-rate dependent. Further details are provided in Appendix A.

https://doi.org/10.5194/egusphere-2025-3036
Preprint. Discussion started: 7 July 2025


### 2.3 Dimensionless parameters and boundary layer thicknesses

Convective heat transfer modelling is widely used in industrial, environmental and Earth Sciences applications over a broad range of spatial and temporal scales. Patterns of convection strongly depend on the geometry, boundary conditions, heat sources and material properties, and they are usually characterized by Rayleigh ($Ra$) and Prandtl ($Pr$) dimensionless numbers. A good review of existing experimental and numerical results in a $Pr - Ra$ representation and convection regimes can be found in Silano et al. (2010). Convection in magmatic chambers is characterized by high $Pr$ and $Ra$ values located in the upper right corner of the regime diagram Fig. 4 from Silano et al. (2010). The corresponding regime is characterized by irregular transient convection, with narrow plumes of hot and cold magma detaching from the upper and lower boundaries between the magma and the host rock. The presence of distinct magmas (basalt and rhyolite) requires fine mesh resolution and expensive computational resources, hence a correct scalability of the problem is needed. Below we estimate the required mesh size in order to resolve the TBL thickness based on the values of parameters listed in Table 1.

| symbol | physical quantity | units | range/initial values |
|---|---|---|---|
| $T$ | Temperature | °C | $T_\infty = 400°, T_o^r = 980°, T_o^b = 1200°$ |
| $T_{ref}$ | Reference Temperature (eq.6) | °C | $T_{ref} = 1000$ |
| $U$ | Velocity | m/s | - |
| $x, y$ | Horizontal & Vertical coordinates | m | - |
| $H$ | Domain size $H \times H$ | m | $H^b = 225, H^r = 750$m |
| $D$ | Intrusion thickness $D$ | m | $D^b = 100, D^r = 300$m |
| $\alpha$ | Thermal expansion (eq.5) | $K^{-1}$ | $3.10^{-5}$ |
| $\tilde{\rho}, \rho_{ref}$ | Local and reference Densities (eq. 5) | $kg/m^3$ | $2300 - 3000$ |
| $\rho_i^{S0}$ | crystal density of $i$ (eq.5) | $kg/m^3$ | $\rho_{S0}^r = 2300, \rho_{S0}^b = 2800$ |
| $\rho_i^{L0}$ | melt density of $i$ (eq.5) | $kg/m^3$ | $\rho_{L0}^r = 2700, \rho_{L0}^b = 3000$ |
| $\kappa_i$ | Thermal conductivity range $i$ | W/m/K | $1 - 2$ |
| $\kappa_o, \kappa_T$ | Thermal conductivity constants (eqs.7) | $W/m/K, K^{-1}$ | $3, 0.002$ |
| $L_*^i$ | Latent heat of crystallization (eqs.7) | J/kg | $3.5 \cdot 10^5$ |
| $Cp_i, Cp_o$ | Heat capacity in $i$ (eqs.7) | J/kg/K | $Cp_o^r = 1200, Cp_o^b = 1000$ |
| $\mu_i = \nu_i.\rho_i$ | Dynamic viscosity | $Pa.s$ | - |
| $\nu_i$ | kinematic viscosity | $m^2/s$ | $0.5 - 10^{12}$, see test cases |

**Table 1.** Variables and Parameters of the models. Indices $^r$ for rhyolite, $^b$ for basalt and $i$ for both recursively.

The Rayleigh number $Ra$ represents the ratio of the buoyancy force to dissipation forces. If $\Delta\rho$ and $\Delta T$ are the density and temperature contrasts across a layer of thickness $H$, $g$ is the gravity acceleration, $k$ is thermal diffusivity and $\mu$ the dynamic

https://doi.org/10.5194/egusphere-2025-3036
Preprint. Discussion started: 7 July 2025


viscosity, $Ra$ can be expressed in two ways:

$$Ra_T = \frac{\rho\alpha g\Delta T H^3}{k\mu}, Ra_\rho = \frac{g\Delta\rho H^3}{k\mu} \tag{9}$$

Prandtl's number characterizes the ratio between the thicknesses of the viscous and the thermal boundary layers, $Pr = \mu C_p/k$. Both scenarios of a hot rhyolite or a hot basalt intrusion are characterized by extremely large $Ra$ and $Pr$ numbers. The intensification of heat transfer with respect to conduction is characterized by the Nusselt number, $Nu = hH/k$, where $h$ is a heat transfer coefficient. The intensity of momentum transfer is characterized by the Reynolds number, $Re = \rho U H/\mu$. At high $Re$ convection is turbulent, while at low $Re$ the flow pattern is laminar but can be highly transient.

Grossmann and Lohse (2000, 2001) theoretically related $Ra - Pr$ and $Nu - Re$ numbers over a wide range of values, and discussed implications on the Boundary Layer (BL) thickness, hence the characteristic length scales $\lambda$ that impose a minimum mesh resolution to the models. They determine $\lambda_U = L/(4\sqrt{Re})$ and $\lambda_T = L/(2Nu)$ as kinematic and thermal length scales, with $Re$ and $Nu$ the Reynolds and Nusselt numbers respectively, and $L = H/2$ the characteristic thickness of the magmatic intrusion. For $Pr > 10^6$, $Nu$ becomes independent of the value of $Pr$ and can be approximated by fitting the data presented on Fig. 2(a) from Grossmann and Lohse (2001) by:

$$\log_{10}(Nu) = 0.0087\log_{10}(Ra)^2 + 0.1350\log_{10}(Ra) - 0.2943. \tag{10}$$

The Reynolds number that corresponds to high $Pr$ and $Ra$ numbers (region $III_\infty$ in Fig. 1 from Grossmann and Lohse (2001)) can be approximated as $Re = 0.015Ra^{2/3}Pr^{-1}$. Table 2 shows characteristic values for typical dimensionless parameters and estimates of the thickness of inertial and thermal boundary layers.

Therefore, we use characteristic density difference $\Delta\rho$ and temperature difference $\Delta T$ that fall between the 50% crystal state

| Parameter | Symbol | Rhyolite | Basalt |
|---|---|---|---|
| Temperature contrast $(°C)$ | $\Delta T$ | 200 | 200 |
| Density contrast $(kg/m^3)$ | $\Delta\rho$ | 200 | 200 |
| Thermal Rayleigh number | $Ra_T$ | $9 \cdot 10^9$ | $2 \cdot 10^{10}$ |
| Compositional Rayleigh number | $Ra_\rho$ | $1 \cdot 10^{11}$ | $2.5 \cdot 10^{11}$ |
| Prandtl number | $Pr$ | $4.9 \cdot 10^8$ | $6.6 \cdot 10^8$ |
| Nusselt number | $Nu$ | 178 | 235 |
| Reynolds number | $Re$ | $6.8 \cdot 10^{-4}$ | $9 \cdot 10^{-4}$ |
| Thermal boundary layer | $\lambda_T$ | 0.42 m | 0.11 m |
| Kinematic boundary layer | $\lambda_U$ | 1436 m | 418 m |

**Table 2.** Estimated dimensionless parameters and minimal thicknesses of the thermal and kinematic boundary layers in rhyolite and in basalt, assuming that relevant variations in temperature and density stand above 50% crystals Marsh (1981). Other parameters taken from Table 1.

and the molten state, for each rhyolite and basalt phase (Marsh, 1981). Analysis of Table 2 reveals that convection is mostly driven by the magma crystallization/melting process, associated with large density variations. $Re$ numbers are small due to

https://doi.org/10.5194/egusphere-2025-3036
Preprint. Discussion started: 7 July 2025


high magma viscosity, meaning that the inertia effects remain insignificant and that the flow is mainly controlled by the competition between the viscous resistance and buoyancy. In turn, the large $Pr$ numbers impose the strongest constraints on the mesh resolution, to resolve the thickness of the thermal boundary layer.

According to Stevens et al. (2013), "*The best way to confirm that the used numerical resolution is sufficient is to obtain the same Nusselt number with different grid resolutions as there is namely always some uncertainty in estimates of the required grid resolution*". We will show that the simulated heat released from the magma becomes mesh-size independent when the mesh size becomes comparable to the width of the TBL.

### 2.4 Numerical Setup and parameter ranges

The model setup is a 2D square domain of dimension $H \times H$ made of rhyolite crust ($r$ subscript parameters) at a uniform temperature of 400°C, in the middle of which a hot magma intrusion of thickness D and Temperature $T_o$ is emplaced (see setup Fig. 3). In scenario 1, the rhyolite intrusion has a thickness $D = 300$ m at temperature $T_o = 980$°C, and the domain's size is $H = 750$ m. In scenario 2, the intrusion is composed of basalt of thickness $D = 100$ m at $T_o = 1200$°C and the domain's size is $H = 225$ m. The top boundary has a free-slip condition while the bottom boundary has a no-slip velocity condition, and temperatures are maintained there, fixed at 400°C. Velocities and temperatures at the lateral borders are set periodic.

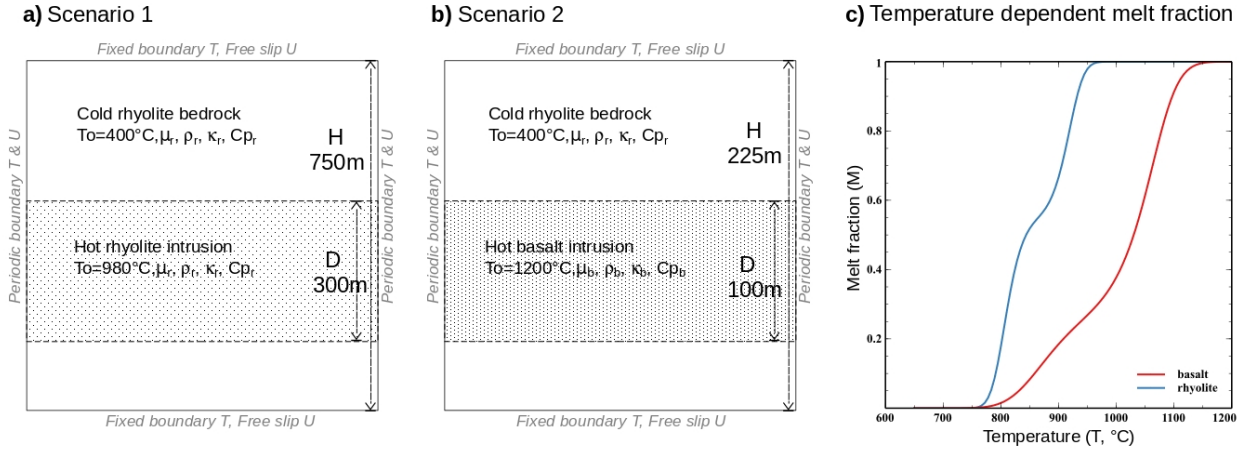


**Figure 3.** Numerical setup for a) a basalt or b) a rhyolite intrusion. Boundary conditions in temperature (T) and velocity (U) displayed in grey. c) melt fraction of magmas depends on temperature according to eqs.(8) for basalt and rhyolite (red and blue curves respectively).

## 3 Model tests and results

The 2D models show how a rhyolite or a basalt intrusion progressively melts the cooler crust above, producing a sharp temperature gradient at the melting front, with the setup provided above (Fig. 3). Complementary tests illustrate the influence of mesh

https://doi.org/10.5194/egusphere-2025-3036
Preprint. Discussion started: 7 July 2025


| Case | Name | size(m)/cells | min($\nu_b - \nu_r$) | max($\nu_b - \nu_r$) | Time | Fig. |
|---|---|---|---|---|---|---|
| R4 | Ryry3LR | 750/182 | 150 | 1e11 | 250y | 6a, B1, |
| R2 | Ryry3 | 750/375 | 150 | 1e11 | 500y | 6a, B1 |
| R1 | Ryry3HR | 750/750 | 150 | 1e11 | 500y | 6a, B1 |
| R0.5 | Ryry3HR2 | 750/1500 | 150 | 1e11 | 250y | 4, 5, 6a, B1 |
| B1.0_v2_m1-10 | NU2LR1 | 300/300 | 2 - 150 | 1e10 - 1e11 | 27y | 6b |
| B0.5_v0.5_m5-50 | K6demip24 | 300/600 | 0.5- 150 | 5e10 - 5e11 | 30y | B3 |
| B0.5_v2_m1-10 | **NU2** | 300/600 | 2 - 150 | 1e10 - 1e11 | 30y | 6b,B1,B3 |
| B0.5_v2_m0.5-0.5 | BWRl3n2m5e9 | 225/450 | 2 - 150 | 5e9 - 5e9 | 40y | B4 |
| B.45_v2_m5-50 | NUDMax11 | 225/500 | 2 - 150 | 5e10 - 5e11 | 30y | 6b,B1,B2,B3 |
| B.45_v10_m1-10 | NU2e1Dx500 | 225/500 | 10 - 150 | 5e10 - 5e11 | 28y | 6b,B3 |
| B.45_v100_m1-10 | NU2e2D | 225/500 | 100 - 150 | 1e10 - 1e11 | 32y | B3 |
| B.45_v1000_m1-10 | NU2nue3 | 225/500 | 1000- 1000 | 1e10 - 1e11 | 65y | B3 |
| B.45_v2_m1-10_x10 | NUall10D | 225/500 | 20-1500 | 1e11 - 1e12 | 40y | 6b,B1,B3 |
| B.45_v2_m1-10_x100 | NUall100D | 225/500 | 200-15000 | 1e12 - 1e13 | 60y | B1,B3 |
| B.25_v2_m1-10 | NU2Dx900 | 225/900 | 2 - 150 | 1e10 - 1e11 | 25y | 6b,7,8,B1 |
| B.25_v10_m1-10 | NU2e1DHR | 225/900 | 10 - 150 | 1e10 - 1e11 | 25y | 6b,B1 |
| B.25_v10_m1-100 | BNUe1DMHR | 225/900 | 10 - 150 | 1e10 - 1e12 | 23y | B1 |
| B.225_v2_m1-10 | X1000NU2A | 225/1000 | 10 - 150 | 1e10 - 1e11 | 12y | 6b, B1 |
| B.225_v10_m1-10 | X1000NU10A | 225/1000 | 10 - 150 | 1e10 - 1e11 | 18y | 6b |
| B.2_v10_m1-100 | NUe1DHR2 | 225/1125 | 10 - 150 | 1e10 - 1e12 | 15y | 6b,B1,B3 |
| B.2_v100_m1-100 | NUe2DHR2 | 225/1125 | 10 - 150 | 1e10 - 1e12 | 13y | 6b,B1,B3 |
| BT20.5_v1_m1-20 | TBAn111 | 250/500 | 1 - 150 | 1e10 - 2e11 | 30y | C1 |
| BT50.4_v2_m5-100 | BTB3 | 200/500 | 2 - 150 | 1e11 - 1e12 | 30y | C2 |

**Table 3.** Model cases, testing the influence of mesh resolution and viscosity ranges. The model name logic is R(meshsize) for Rhyolite cases and B(meshsize)_v(vismin)_m(vismax) for basalt intrusion cases, with "vismin" the minimum basalt viscosity and "vismax" the maximum basalt-maximum rhyolite viscosities factor of $10^{10} m^2/s$. The case in bold is the reference case for a basalt intrusion. The last two cases test the basaltic sill thickness (20 m and 50 m). "Time" is the maximum time until which the model could run.

resolutions, viscosities, and domain sizes on the evolution of this melting front; they are listed in Table 3 and are described in greater detail in Appendix B. Here we present the results around a main best resolution case for each scenario, and synthesize the importance of these numerical artifacts. A comparison with a 1D model complements this analysis.

### 3.1 2D Rhyolitic sill intrusion (scenario 1)

Our first scenario considers the injection of a rhyolitic sill. Figure 4 displays snapshots in time of the temperature, melt fraction and velocity, and zooms of other variables near the melting front. Figure 5 displays the temporal evolution of the melting front, velocity and averaged temperature profiles. Since the hot intrusion domain is initially set at 980°C, it convects. Over time,

https://doi.org/10.5194/egusphere-2025-3036
Preprint. Discussion started: 7 July 2025


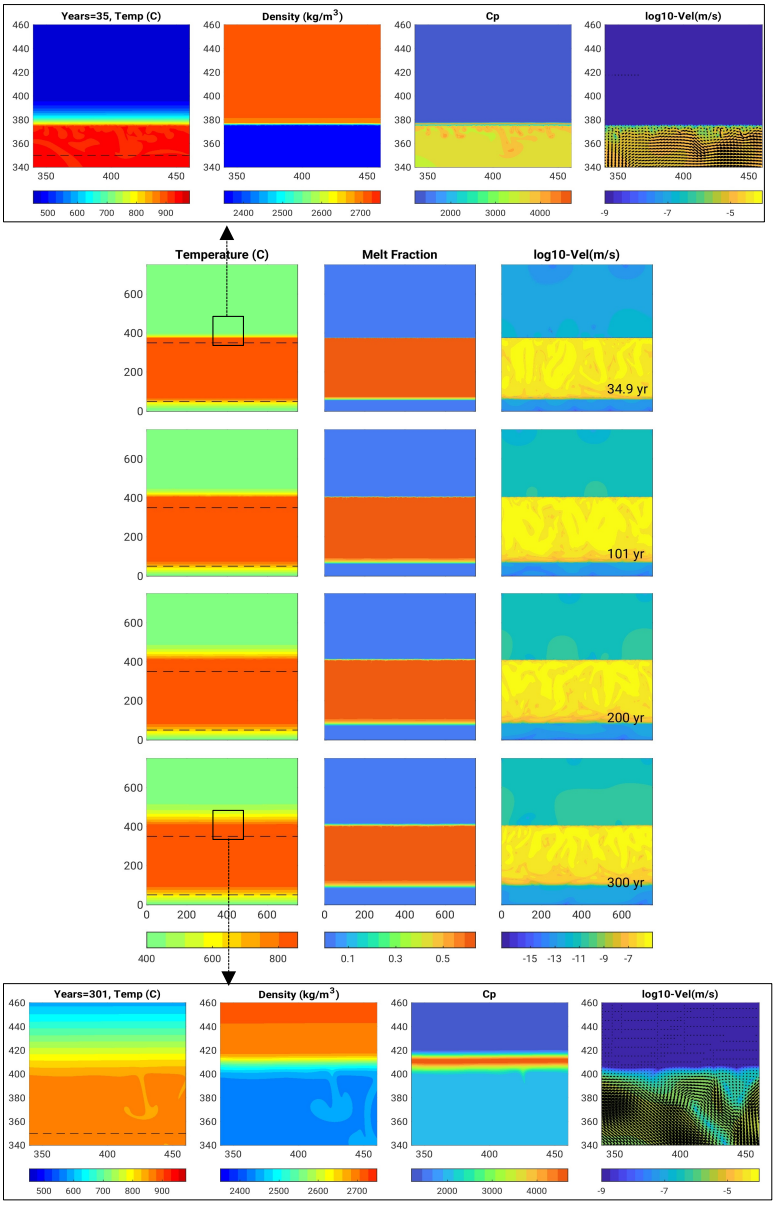


**Figure 4.** Rhyolite intrusion 300 m thick (scenario 1, model R0.5): In the centre, there are snapshots in time of the temperature (left column), melt fraction (middle) and velocity field (right) over the entire domain size. Dashed lines indicate the initial location of the hot intrusion, and help see heat propagating upwards, together with the melting front and the velocity field. Figures in boxes on the top and bottom are close-ups near the upper melting front displaying temperature, density, heat capacity, velocity after 35 and 300 yr, respectively.

https://doi.org/10.5194/egusphere-2025-3036
Preprint. Discussion started: 7 July 2025


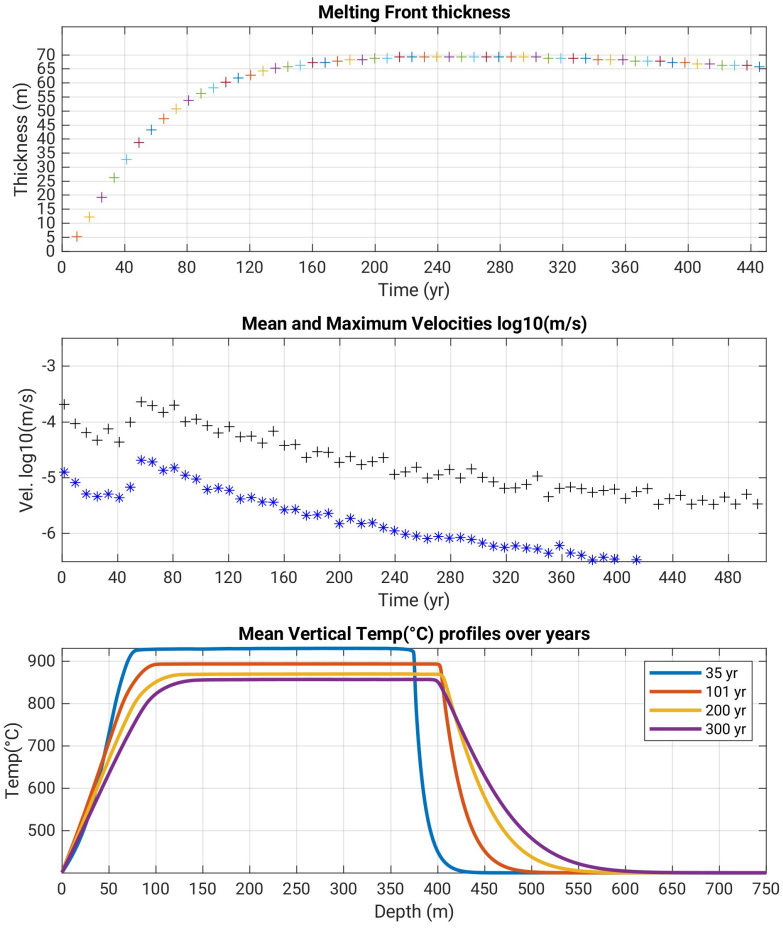


**Figure 5.** Rhyolite intrusion (scenario 1, model R0.5): Melt front thickness (top, thickness over the initial emplacement depth at y=350 m) and velocities (middle, in $log_{10}$ scale) over time, and average temperature profiles with depth (bottom). Note that the melting front thickness starts to decrease from ca. 300 yr; the 400°C jump occurs over 30 m after 35 yrs, then over more than 100 m after 300 yrs after emplacement.

this domain progressively "shifts" upwards, with the rhyolite melting front propagating upwards and the base of the intrusion cooling down and adopting a conductive regime. This model illustrates the following key features of heat transfer:

- The melting front propagates upwards reaching an additional thickness of about 15 m after 35 years, and 70 m after 200 years following intrusion emplacement.
- After 35 years, a temperature gradient of 450°C occurs over a depth range of about 30 m (between depths 370 and 400 m, Fig.4). After 300 years, this temperature jump occurs over a depth range of more than 150 m.

The melting front boundary develops sharp density, conductivity and heat capacity gradients. After 35 years these contrasts reach ca. 10% for the conductivity, 16% for the density, and 50% for the heat capacity (Figure 4, top). After 300 years the

https://doi.org/10.5194/egusphere-2025-3036
Preprint. Discussion started: 7 July 2025


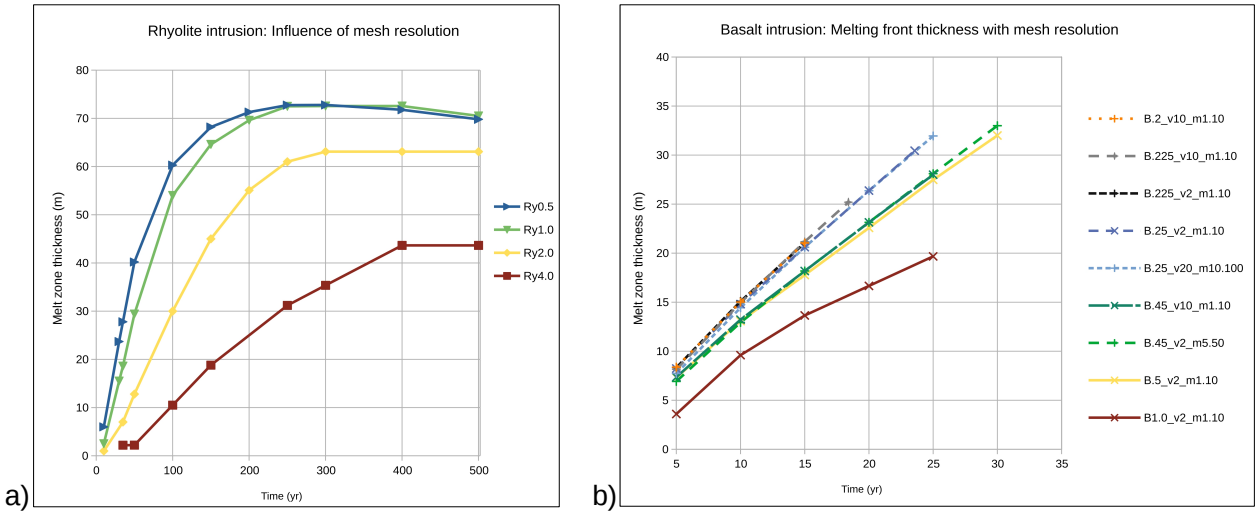


**Figure 6.** Mesh resolution tests for a) a rhyolite intrusion (scenario 1) and b) a basalt intrusion (scenario 2): melt zone thickness over time with respect to its initial top location. Numbers in legend refer to cell size and viscosities, see Table 3 for further details. The model cases in blue are the ones displayed in Figs. 4, 5, 7 and 8.

domain of molten rhyolite has shifted up by 75 m, but the system is cooling down with much smoother temperature gradient, density and conductivity gradients (Figure 4, bottom). Heat capacity still varies greatly due to the influence of latent heat, but over a thinner ∼10 m thick layer. The molten zone starts to shrink down to ca. 70 m from about 320 years (Figure 5).

Comparison of the melting zone thickness (MZT) over time for different mesh resolutions is illustrated in Figure 6a. We see that for mesh sizes smaller than 1 m, the MZT evolves close to each other with differences reaching 20% (12 m) after ca. 50 years, but decreasing to less than ca. 2% after 100 years. We propose that critical mesh size has been reached and that the heat transfer is modelled correctly.

During the IDDP-1 experiment, the temperature increased by more than 100°C over several meters: in comparison in this modelled scenario 1, the temperature increases by about 450°C over about 30 m (15°C/m), 35 years after emplacement of the intrusion (e.g., assuming emplacement during the 1984 Krafla fires). This is just about equal to the gradient that was observed. It becomes more difficult to attribute the observed thermal gradient to a rhyolite body intruded 300 years ago, since the model indicates that the sharp thermal gradient then spreads over a thickness of 150 m, corresponding to a temperature increase of 3°C/m (Figure 5, bottom). Hence the motivation to attempt a model case with a basaltic intrusion, cf. next section.

### 3.2 2D Basaltic sill intrusion into felsic crust (scenario 2)

For scenario 2 we assume that a basaltic sill of 100 m at 1200°C is injected into cold rhyolite crust. The results are displayed in Figures 7 and 8: in Figure 7 the thermal gradient between molten basalt and cold rhyolite (the dashed line represents its initial

https://doi.org/10.5194/egusphere-2025-3036
Preprint. Discussion started: 7 July 2025


location), shows how the rhyolite layer progressively melts, with "independent" convection developing between the convecting basaltic layer and the conductive host rock above.

Figure 7 shows that a layer of partially molten granophyre (rhyolite) has already formed 5 years after injection, and it expands steadily during the following decades. Within that layer, the density contrast reaches 500 kg/m$^3$ and heat capacity is boosted by latent heat, exceeding in effect values of 4000 J/K. Velocities are slow at the beginning and then increase and vary with spikes related to the convection dynamics (Figure 8). From about 15 yrs onwards we see that the velocities start to reduce, indicating that the maximum rate of heat transfer has passed; the system cools down despite the melting zone thickness (MZT) still increases. The initially sharp thermal jump at the basalt-rhyolite boundary forms a plateau (which represents the convective layer of partially molten rhyolite). Ultimately, this plateau will smooth out towards a conductive profile over time (cf. Figure 8):

- After 5 years, the temperature jump across molten/unmolten rhyolite evolves from about 500 to 1000°C over a depth range of about 10 m (between depths ca. 160 to 170 m), which corresponds to a thermal gradient of 50°C/m,
- After 25 years (Fig.7c), the temperature evolves from 500 to 950°C over ca. 20 m, which corresponds to a thermal gradient of about 25°C/m/m.
- The melting front thickness (the plateau) reaches ca. 30 m after 23 years, and still displays an increasing trend.

This rather high resolution case crashed after 25 years. We conducted a number of additional tests with even less success. Naturally, lower resolution tests were faster computationally and could run for longer times, but lost accuracy. Figure 6b displays the MZT evolution for our most successful attempts, and confirms the first-order influence of the mesh cell sizes on melting front propagation rates. However a tendency can be drawn: the difference in mesh cell sizes between 0.5 m and 1 m reaches 25% (MZT 20 m vs. 27 m); it reduces to 15% between 0.25 m and 0.5 m (MZT 27 m vs. 32 m), after 25 yr. Models at cell size 0.2 m could not exceed a total time duration of 15 yr, and differ by 3% from those at mesh size 0.25 m. This indicates that despite considering mesh sizes twice larger than the required critical mesh size (cf. section 3), the MZT is underestimated by less than 30% in the case of a resolution ratio of 0.25 after 20 yr (when the system's velocities already decrease, see further details in Appendix B). Therefore one can expect it would actually reach at most double thickness if we could reach the critical mesh size. Extrapolating time for another 15 years (up to 35 years) leads to an additional MZT of 15 m, which allows us to propose that the melt front thickness reaches $50 \pm 10$ m thick, 35 yrs after emplacement (after the Krafla Fires).

Additional tests of the modelled domain size and minimum or maximum viscosity are displayed in Appendix B, and show how the melting front thickness (MZT) is affected in the following ways:

- Tests with a wider domain ($500 \times 600$ m) show no significant difference with the reference case ($225 \times 225$ m), indicating that the chosen model height and width do not influence the results (Appendix Fig. B3a).
- Higher maximum viscosities for both rhyolite and basalt domains have a minor effect on the results, within a range of values of $10^{10} - 10^{12}$ m/s. Greater values do not impact the system's dynamics given its overall time-scale, and lower rhyolite viscosity destabilizes the system but does not appear physically realistic.

https://doi.org/10.5194/egusphere-2025-3036
Preprint. Discussion started: 7 July 2025


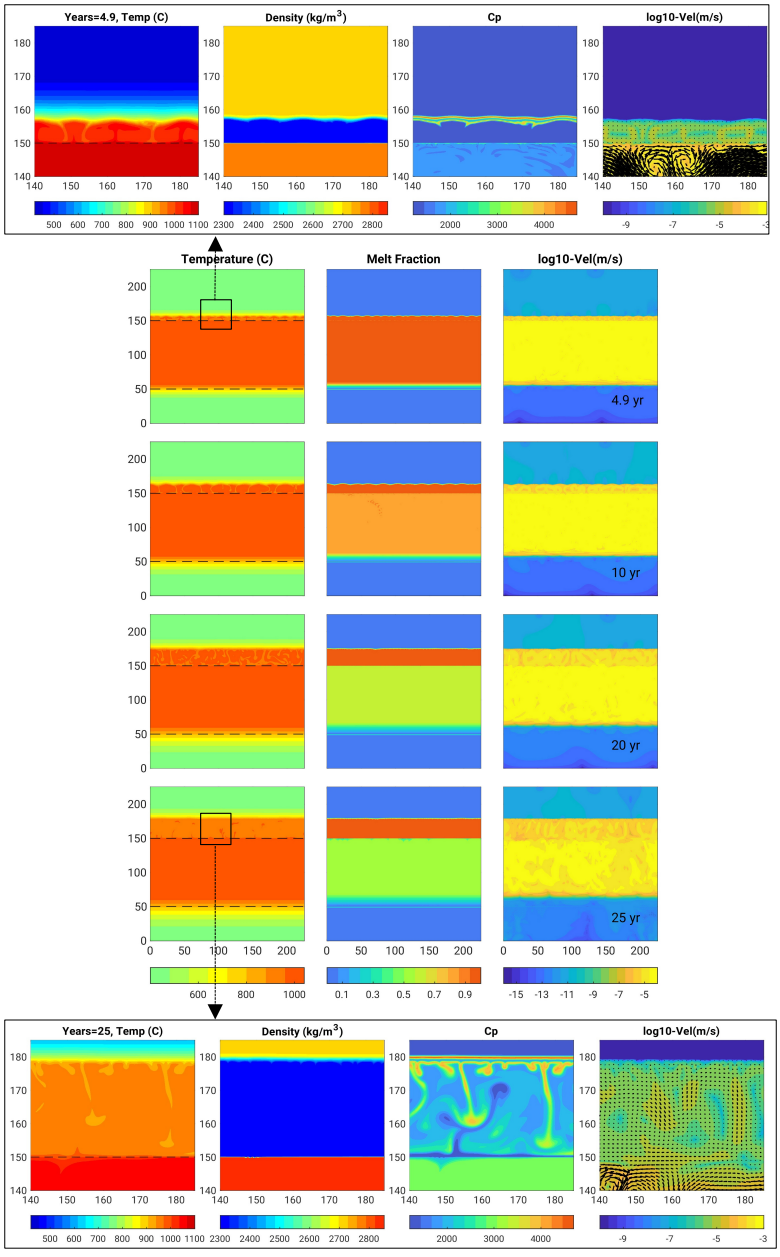


**Figure 7.** 2D Model with a basalt intrusion (scenario 2, model B.25_v2_m1-10): center figures show snapshots in time of temperature (left), melt fraction (middle) and velocity field (right). The dashed lines represent the initial upper boundary of the intrusion. Top-bottom figures zoom at the melting front boundary: temperature, density, heat capacity and velocity, after 10, 20 and 25 yr.

https://doi.org/10.5194/egusphere-2025-3036
Preprint. Discussion started: 7 July 2025


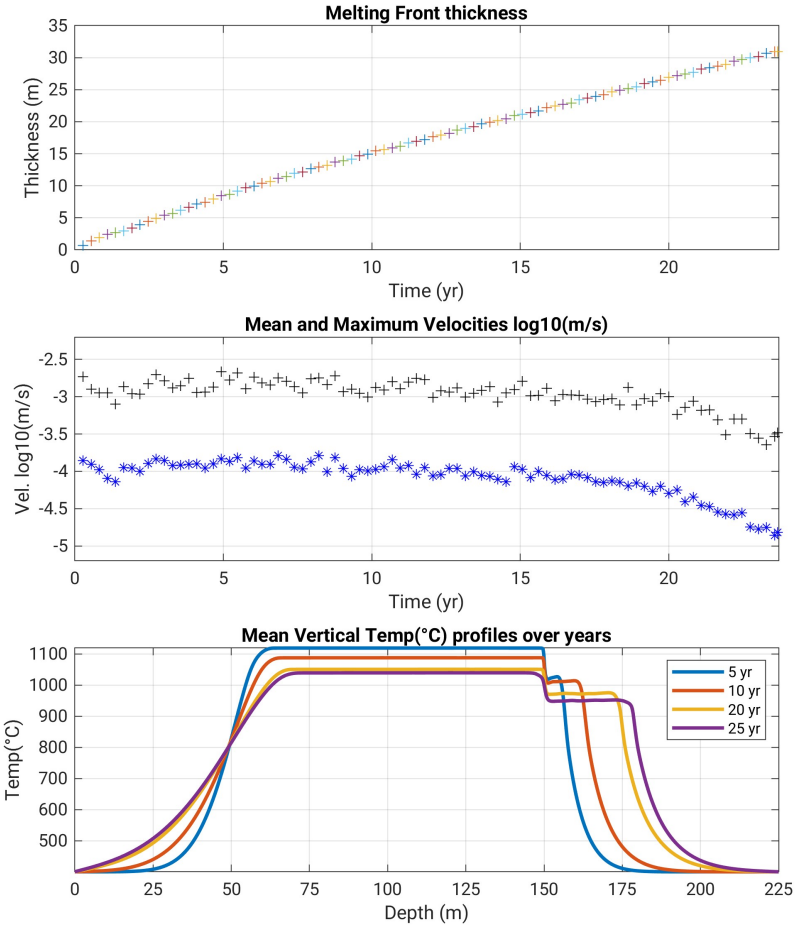


**Figure 8.** Basalt intrusion (scenario 2): Melt zone thickness and velocities over time, and average temperature profiles with depth.

– We also tested the minimum viscosity (for basalt), since it affects the numerical time-step (reducing it reduces the time-step). Our comparisons in Appendix Fig. B3 show that the melt front propagation rate and the system's velocities vary by less than 10% when the minimum kinematic viscosity ranges from 0.5 to 10 $m^2/s$. The melting zone thickness and the velocities are reduced by about 20% when the minimum viscosity is multiplied by a factor of 50.

Since the numerical mesh resolution has a strong impact on the modelled results, the 2D reference case is further compared with a 1D study in the next section.

### 3.3 Comparison between 2D simulations and a simplified 1D model

Modifying the approach of Huppert and Sparks (1988), Borisova et al. (2023) developed a 1D thermochemical model of heat transfer from a convecting basaltic intrusion into host felsic rocks, reproducing its melting and the production of hot rhyolite

https://doi.org/10.5194/egusphere-2025-3036
Preprint. Discussion started: 7 July 2025


magma. This 1D thermochemical model is based on a non-linear heat conduction equation which accounts for the release of latent heat of crystallization and for convection (via effective thermal conductivity) in a three-layered system with contrasting compositions. The middle layer contains initially hot basaltic magma that releases heat and melts the surrounding felsic rocks. We use the same phase diagrams and rheological models for basalt and rhyolite as in the full 2D simulations. The model is described by the following system of equations for each layer $i = 1, 3$:

$$\begin{aligned} &\rho_i Cp_i \frac{\partial T}{\partial t} = \frac{\partial}{\partial x}\kappa_i \frac{\partial T}{\partial x}; Cp_i = Cp_i^0 + \frac{dX_i}{dT} L_*^i; \\ &Nu_i = \frac{Q_{conv}}{Q_{cond}} = G(Ra_i); \kappa_i = \kappa_m(T) \cdot Nu_i \end{aligned} \tag{11}$$

Here the dependence of the $Nu$ number on the $Ra$ number ($G(Ra_i)$) is described by eq. (10). $\kappa_m(T)$ is the molecular (or local) conductivity.

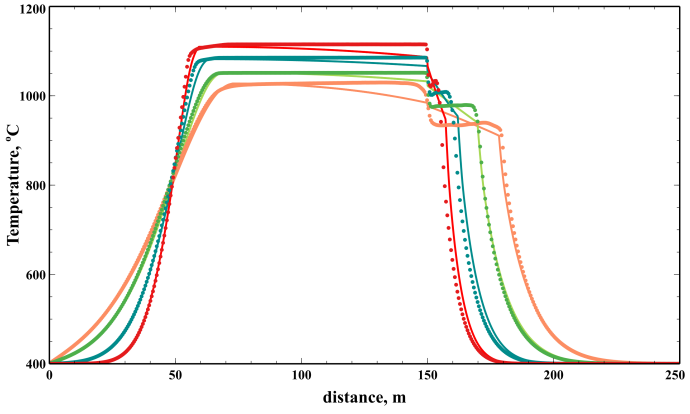


**Figure 9.** Comparison between 2D (dots) and 1D (solid line) averaged temperatures at 5, 10, 20 and 30 years, for the basaltic intrusion (scenario 2).

Each layer is divided into several zones representing thermal boundary layers and the core of the flow, where intense convective mixing occurs. According to 2D simulations very little melting occurs at the bottom contact between basaltic magma and the crust. Instead, the solidification front propagates in basaltic magma leading to a decrease in the effective width of the convective layer. We use the analytical solution of Stefan's problem to calculate the position of this front as:

$$x_s = \sqrt{\frac{k \cdot t}{Ste}}, Ste = \frac{Cp^b \Delta T}{L_*^b} \tag{12}$$

where $\Delta T = 300$ K gives the best fit to the front position (see Fig. 9).

In the middle of the convective layers the effective thermal conductivity is parametrized based on the $Nu - Ra$ relationship approximated by fitting the data from Grossmann and Lohse (2001) for extremely large $Pr$ numbers, cf. eq. 10 (section 2).

Fig. 10 shows that after the intrusion of basaltic magma the effective thermal conductivity can exceed the "molecular" thermal conductivity by up to 3 orders of magnitude. This leads to a uniform temperature distribution within the molten magma. As the basaltic layer cools down the value of effective conductivity decreases progressively. At the upper contact between basaltic

https://doi.org/10.5194/egusphere-2025-3036
Preprint. Discussion started: 7 July 2025


magma and molten rhyolite, two TBLs are formed in both magmas. Their thicknesses are calculated using the assumption that the $Ra_\delta$ number defined by the thickness of the TBL $\delta$ is equal to the critical value, $Ra_* = 1708$ for the onset of convection in a horizontal layer. The same TBL originates at the boundary between molten rhyolite and the host rock which is defined by the position of the maximum value of the temperature gradient $\frac{\partial T}{\partial x}$.

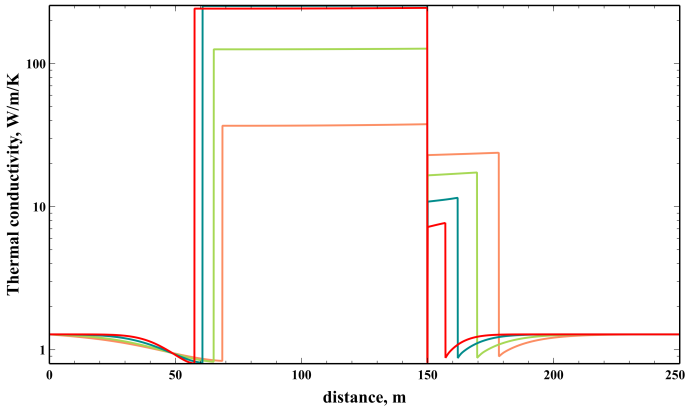


**Figure 10.** Effective thermal conductivity at 5, 10, 20 and 30 years.

Overall, there is good agreement between the predictions of the 1D and 2D models, although the 1D model shows temperature gradients within convective regions, meaning that the estimated value of the effective thermal conductivity is not large enough. That might be a consequence of strain-rate dependent viscosity used in the 2D modeling, while the 1D modeling uses an averaged value. The high $Nu$ numbers obtained in the 1D simulations are close to the values shown in Table 2, suggesting that both 1D and 2D models capture the convective heat transfer correctly.

## 4 Discussion

In this work, for the two modelled scenarios of the cooling of a basaltic or rhyolite intrusion, we have obtained a propagating melting front through initially cold rhyolite within ca. 30 years or more, that displayed sharper temperature gradients in case of a basaltic intrusion than in case of a rhyolitic intrusion. Several aspects of this modelling are discussed below, separated into numerical aspects first and then aspects related to petrological observations from Krafla.

### 4.1 Numerical aspects and potential complementary factors at play

We have tested the influence of the numerical mesh size, and concluded that in case of a rhyolitic intrusion we achieved a mesh size (50 cm) that approaches sufficiently the minimal thickness of the thermal boundary layer (40 cm), and therefore we believe we produce realistic results, within 10% error. In case of the basaltic intrusion our highest resolution (20 cm) is still twice larger than the theoretical thickness of the boundary layer (11 cm, cf. Table 2) and our comparisons show that the melting

https://doi.org/10.5194/egusphere-2025-3036
Preprint. Discussion started: 7 July 2025


zone thickness is still likely underestimated, but by less than a factor of 2. Hence we predict an upper bound of 60 m for the MZT for 100 m thick initial intrusion.

We could have also tested a variety of intrusion thicknesses and more complicated shapes than just a flat layer, a three-dimensional body instead of an infinitely long layer as implied by the 2D assumption; this would also affect the melting front thickness by a comparable amount. The intrusion's thickness is actually not well constrained by geophysical data below Krafla, and obviously it also controls the amount of melting of the overlying rhyolite. We chose an a priori value of basalt thickness of 100 m, based on previous estimates by e.g., Borisova et al. (2023). We display in Appendix C, two extra cases with a 20 m thick and 50 m thick basalt intrusion. The 20 m thick intrusion appears too thin to generate convection in the overlying rhyolite (Figure C1) and the thermal profile remains conductive in that case. The 50 m thick intrusion generates convection within 20 m of partially melting rhyolite (Figure C2), and a reasonable temperature jump compared to observations. Hence a basaltic sill 50 m thick can also be a realistic scenario.

In order to approach the required mesh size in our models, many cases actually crashed and to achieve reasonable modelled time duration, we had to increase the minimum viscosity in order to handle greater numerical time-steps. Therefore we tested the influence of the viscosity ranges; while the minimal viscosity of rhyolite is well constrained and did not require testing, that of basalt had to be multiplied by a factor of 2 or 10 in order to achieve greater modelled times. We discussed and showed in Appendix B, that below a kinematic viscosity of 10 $m^2/s$ the results display similar behaviour and similar melting front propagation rates. Besides, augmenting the maximum viscosity does not have a significant impact, given that the modelled time durations are shorter than the typical time scale of the problem. On the other hand, a model in which the host rock maximum viscosity was reduced by a factor of 5 (Fig. B4) showed that the partially molten host rock destabilizes gravitationally within about 20 years, producing diapirism and a significantly smoother temperature gradient than the one observed during the IDDP-1 drilling. By elimination, this extreme case shows that our choice of maximum viscosity of the host rock in the other models was sufficient.

Finally, one may ask whether the active hydrothermal system above Krafla's magma reservoir influences the evolution of the melting processes modelled here. In fact, the water content of Krafla's fresh lavas to granophyres is low and of the order of 0.1 to 1.2 wt% $H_2O$, and the crustal rocks are strongly heterogeneous with respect to $^{18}O_{VSMOW}$ (Borisova et al., 2024). Thus, the felsic glassy samples from IDDP-1 and KJ-39 are nearly anhydrous, indicating that meteoric fluids participated in the origin of these crustal rocks which were re-crystallized or quenched at shallow depth. Thus, hydrothermal circulation in the crust does not play a direct role in its partial melting and the following reaction of the rock with basaltic magma. Nevertheless, the thermo-mechanical-chemical coupling between the hydrothermal and magmatic domains is known to be complex, and most advanced modelling studies still rely on strong assumptions such as empirical thresholds for crystal content and/or permeability, which are difficult to precisely constrain in the field (e.g. Gruzdeva et al., 2024).

The geothermal gradient obtained in our study reaches 28°C/m after 25 to 30 years of basalt-rhyolite interaction; in order to explain potentially even greater geothermal gradients, one would need to take into account more localized, reactive fluid flow processes, such as reactive porosity waves (Wong and Keller, 2023), brittle behavior (Witcher et al., 2025) or specific

https://doi.org/10.5194/egusphere-2025-3036
Preprint. Discussion started: 7 July 2025


drilling-induced localized flow (Wadsworth et al., 2024). A full complementary "THMC" (thermo-hydro-mechanical-chemical) modeling study will then be needed to tackle the magma dynamics below Krafla, hopefully in the near future.

### 4.2 Complementary arguments from analyses of Krafla's rock samples

From the two principal scenarios that were simulated here, the numerical results indicate that the 'basaltic intrusion' scenario best matches the temperature jump observed during the IDDP-1 drilling experiment, in association with a propagating melting front that separates convective and conductive heat transfer modes. With a basaltic magma intrusion the density contrast between the intruded magma and the molten host rock remains high, prevents intense mixing, and a two-layer convection structure forms as shown in Figure 7. We prefer this scenario to the one assuming a rhyolitic melt intrusion.

The main question about basaltic versus rhyolitic intrusions interacting with the Icelandic crust is still debated, although our previous study (Borisova et al., 2023) and the current investigation of the Krafla zero-age material (IDDP-1 and KJ-39 samples Borisova et al., 2024) suggest a direct participation of basaltic rather than rhyolitic magma in the production of the felsic samples drilled. Our thermodynamic modelling of equilibrium crystallization of the Krafla granophyre (or felsite) performed using rhyolite-MELTS (Borisova et al., 2024) at 900–1150 $^{O}$C predicts that clinopyroxene, orthopyroxene, sodic plagioclase $An_{10\text{-}20}$, K-feldspar, quartz and magnetite spinel, rutile are stable at 0.1 GPa and at the QFM (quartz-fayalite-magnetite) buffer. These mineral phases (except for rutile) are observed in the Krafla felsite samples and IDDP-1 glassy samples, suggesting that they attained physical-chemical conditions close to thermodynamic equilibrium due to high degrees of partial melting. These evidences are also in agreement with experimental data on partial melting of the Krafla granophyre (Masotta et al., 2018).

From a petrological point of view, the interaction of basaltic magma with felsite or granophyre crust is recorded by the presence of accessory mineral phases, such as baddeleyite, together with zircon and chevkinite and by significant glass heterogeneity with respect to Si, Fe, Ca and $^{18}O_{VSMOW}$ in the IDDP-1 and KJ-39 samples drilled (Borisova et al., 2024). The model can be completed by the available oxygen isotope data; as shown by Hampton et al. (2021), the low $\delta^{18}O_{VSMOW}$ (+3‰) measured in the IDDP-1 samples cannot have formed due to segregation of pure partial melt alone, and they also require assimilation and/or further fractional crystallization.

The magmatic crystals in the Víti felsite appear almost mantle-like (e.g., pyroxene IC-82; +4.75‰), while others have much lower $^{18}O_{VSMOW}$ values that appear to reflect assimilation of hydrothermally altered material (e.g. plagioclase IC-83; -5.35‰). This strong isotopic heterogeneity can be directly explained by multi-stage granophyre rock-basalt-fluid interaction, where hydrothermal fluid-altered granophyre rocks have heterogeneous $\delta^{18}O$ (below 0‰) and the basaltic source has mantle signatures ( 5‰ $\delta^{18}O$). As stated above, different batches of silicic melts were likely produced during the partial melting of the host granophyre rocks which are strongly heterogeneous due to the effect of hydrothermal fluids. Thus, the partial melting of quartz-feldspar-rich granophyre rock and the related hybridization with basalt provide the main control on the composition of the hybrid magma, recording significant compositional variations. In this context, the 1975–1984 Krafla Fires basaltic eruption constrains the time of the IDDP-1 rhyolite magma emplacement to the previous 33 years.

https://doi.org/10.5194/egusphere-2025-3036
Preprint. Discussion started: 7 July 2025


## 5 Conclusions

In this work, we have modelled in two dimensions the cooling of a basaltic and a rhyolite intrusion over decades, and we have obtained a propagating melting front through the initially cold rhyolite above it: the models display sharper temperature gradients in case of a basaltic intrusion than in the case of a rhyolitic intrusion. This finding corroborates other petrological arguments that indicate that the 2009 IDDP-1 experiment at Krafla drilled into felsic crust that was molten in contact with a basaltic intrusion from below. Cooling of a rhyolitic intrusion over 300 years produces a much smoother thermal gradient, insufficient to explain the 2009 IDDP-1 observations. These results allow us to rule out the scenario in which the intrusion would have been emplaced 300 years ago during the Myvatn Fires, and instead favour its emplacement during the Krafla Fires.

Although these models only approach the limit of the numerical resolution of the boundary layer of the convecting partially molten domain, they allow us to evaluate the thickness of the melting zone within the 33 years after the Krafla Fires; we obtain values near 30 meters which can be multiplied by two considering both physical unknowns and numerical mesh-size limitations.

These results offer useful information given the other uncertainties such as the initial intrusion thickness or hydrothermal effects, for which next generation models accounting for multiphase flow will be best appropriate.

*Code availability.* The OpenFOAM solver, reference case input files and movie are available here (upon signing in): https://gitlab.com/AurelieLN/MultiMeltInterFoam. See the associated user guide for further details.

*Data availability.* All data is presented in the main text of the paper and appendixes

*Author contributions.* Conceptualization: OM, MG, AB. Formal analysis: MG,OM. Funding acquisition: AB. Investigation: MG, OM, AB. Methodology: OM, MG. Software: MG,OM. Resources: AB. Writing of the original draft: OM, MG, AB. Writing review and editing: OM, MG, AB.

*Competing interests.* The authors declare that they have no conflict of interest

https://doi.org/10.5194/egusphere-2025-3036
Preprint. Discussion started: 7 July 2025


*Acknowledgements.* This work was supported by the program PAUSE from Collège de France, the PLAGIOGRAN INSU-SYSTER project, and a Visiting Professor position for O.M. from Toulouse University. This article is funded by the European Union (ERC, PLANETAFELSIC, project 101141259) to A.B. Views and opinions expressed are however those of the author(s) only and do not necessarily reflect those of the European Union or the European Research Council. Neither the European Union nor the granting authority can be held responsible for them. Numerical models were carried out on the CNRS regional supercomputer center CALMIP (https://www.calmip.univ-toulouse.fr/) under project number *p24041*. AnneMarie Cousin (GET) drew Figure 1. Discussions with Simon Rooyakkers (GNS) and Thomas Bonometti (IMFT) greatly helped mature the study.

https://doi.org/10.5194/egusphere-2025-3036
Preprint. Discussion started: 7 July 2025


## References

Berberović, E., van Hinsberg, N. P., Jakirlić, S., Roisman, I. V., and Tropea, C.: Drop impact onto a liquid layer of finite thickness: Dynamics of the cavity evolution, Physical Review E, 79, 036 306, https://doi.org/10.1103/PhysRevE.79.036306, 2009.

Borisova, A. Y., Bohrson, W. A., and Spera, F. J.: Magma-Rock and Magma-Mush interactions as fundamental processes of magmatic differentiation, 2021.

Borisova, A. Y., Melnik, O. E., Gaborit, N., Bindeman, I. N., Traillou, T., Raffarin, M., Stefansson, A., Laurent, O., Leisen, M., et al.: In situ probing of the present day zircon bearing magma chamber at Krafla, Northeastern Iceland, Frontiers in Earth Science, 11, 1307 303, 2023.

Borisova, A. Y., Bindeman, I. N., Kennedy, B., Alex, N., Gaborit, N., Brianna, K., Georgina, R., Stefánsson, A., et al.: Experimental investigation of basaltic melt-felsic crust reaction: Implications for zero-age rhyolite genesis and felsic crust reworking, in: AGU 2024, vol. 11, 2024.

Carrigan, C. R.: Time and temperature dependent convection models of cooling reservoirs: Application to volcanic sills, Geophys. Res. Lett., 11, 693–696, 1984.

Costa, A., Caricchi, L., and Bagdassarov, N.: A model for the rheology of particle-bearing suspensions and partially molten rocks, Geochemistry, Geophysics, Geosystems, 10, 2009.

Eichelberger, J.: Distribution and transport of thermal energy within magma hydrothermal systems, Geosciences, 10, 212, 2020.

Eichelberger, J., Carrigan, C., Ingolfsson, H. P., Lavallée, Y., Ludden, J., Markusson, S., et al.: Magma-sourced geothermal energy and plans for Krafla Magma Testbed, Iceland, in: Proceedings World Geotherm Congress, vol. 1, p. 2021, 2020.

Einarsson, P.: S-wave shadows in the Krafla caldera in NE-Iceland, evidence for a magma chamber in the crust, Bulletin Volcanologique, 41, 187–195, 1978.

Giordano, D., Russell, J. K., and Dingwell, D. B.: Viscosity of magmatic liquids: a model, Earth Planet. Sc. Lett., 271, 123–134, 2008.

Grönvold, K. and Mäkipää, H.: Chemical composition of Krafla lavas 1975-1977, 1978.

Grossmann, S. and Lohse, D.: Scaling in thermal convection: a unifying theory, Journal of Fluid Mechanics, 407, 27–56, 2000.

Grossmann, S. and Lohse, D.: Thermal convection for large Prandtl numbers, Physical review letters, 86, 3316, 2001.

Gruzdeva, Y., Weis, P., and Andersen, C.: Timing of volatile degassing from hydrous upper-crustal magma reservoirs with implications for porphyry copper deposits, Journal of Geophysical Research: Solid Earth, 129, e2023JB028 433, 2024.

Gualda, G. A., Ghiorso, M. S., Lemons, R. V., and Carley, T. L.: Rhyolite-MELTS: a modified calibration of MELTS optimized for silica-rich, fluid-bearing magmatic systems, Journal of Petrology, 53, 875–890, 2012.

Hampton, R., Bindeman, I., Stern, R., Coble, M., and Rooyakkers, S.: A microanalytical oxygen isotopic and U-Th geochronologic investigation and modeling of rhyolite petrogenesis at the Krafla Central Volcano, Iceland, Journal of Volcanology and Geothermal Research, 414, 107 229, 2021.

Hollingsworth, J., Leprince, S., Ayoub, F., and Avouac, J.-P.: Deformation during the 1975–1984 Krafla rifting crisis, NE Iceland, measured from historical optical imagery, Journal of Geophysical Research: Solid Earth, 117, 2012.

Huppert, H. E. and Sparks, R. S. J.: Melting the roof of a chamber containing a hot, turbulently convecting fluid, J. Fluid Mechanics, 188, 107–131, https://doi.org/10.1017/S0022112088000655, 1988.

Kim, D., Brown, L. D., Árnason, K., Gudmundsson, Ó., Ágústsson, K., and Flóvenz, Ó. G.: Magma "bright spots" mapped beneath Krafla, Iceland, using RVSP imaging of reflected waves from microearthquakes, Journal of Volcanology and Geothermal Research, 391, 106 365, 2020.

https://doi.org/10.5194/egusphere-2025-3036
Preprint. Discussion started: 7 July 2025


Louis-Napoleon, A., Gerbault, M., Bonometti, T., Thieulot, C., Martin, R., and Vanderhaeghe, O.: 3-D numerical modelling of crustal polydiapirs with Volume-Of-Fluid methods, Geophys. J. Int., 222, 474–506, 2020.

Louis-Napoleon, A., Bonometti, T., Gerbault, M., Martin, R., and Vanderhaeghe, O.: Models of convection and segregation in heterogeneous partially molten crustal roots with a VOF method- part I: flow regimes, Geophys. J. Int., 229, 2047–2080, 2022.

Louis-Napoléon, A., Gerbault, M., Bonometti, T., Vanderhaeghe, O., Roland, M., and Maury, N.: Convection and segregation in heterogeneous orogenic crust with a VOF method - Part II: how to form migmatite domes, Geophys. J. Int., p. ggad388, 2024.

Marsh, B.: On the crystallinity, probability of occurrence, and rheology of lava and magma, Contributions to Mineralogy and Petrology, 78, 85–98, 1981.

Masotta, M., Mollo, S., Nazzari, M., Tecchiato, V., Scarlato, P., Papale, P., and Bachmann, O.: Crystallization and partial melting of rhyolite and felsite rocks at Krafla volcano: A comparative approach based on mineral and glass chemistry of natural and experimental products, Chemical Geology, 483, 603–618, 2018.

Mbia, P. K., Mortensen, A., Oskarsson, N., and Hardarson, B.: Sub surface geology, petrology and hydrothermal alteration of Menengai geothermal field, Kenya, United Nations University, 2014.

Mortensen, A., Grönvold, K., Gudmundsson, Á., Steingrímsson, B., and Egilson, T.: Quenched silicic glass from well KJ-39 in Krafla, North-Eastern Iceland, in: World Geothermal Congress, pp. 1–6, 2010.

Mortensen, A., Egilson, T., Gautason, B., Árnadóttir, S., and Gudhmundsson, Á.: Stratigraphy, alteration mineralogy, permeability and temperature conditions of well IDDP-1, Krafla, NE-Iceland, Geothermics, 49, 31–41, 2014.

Rooyakkers, S. M., Stix, J., Berlo, K., Petrelli, M., Hampton, R. L., Barker, S. J., and Morgavi, D.: The origin of rhyolitic magmas at Krafla Central Volcano (Iceland), J. Petrology, 62, egab064, 2021.

Rooyakkers, S. M., Carroll, K. J., Gutai, A. F., Winpenny, B., Bali, E., Guðfinnsson, G. H., Maclennan, J., Sigmundsson, F., Jónasson, K., Mutch, E. J., et al.: Hydraulically linked reservoirs simultaneously fed the 1975–1984 Krafla Fires eruptions: Insights from petrochemistry, Earth and Planetary Science Letters, 646, 118 960, 2024.

Schuler, J., Greenfield, T., White, R. S., Roecker, S. W., Brandsdóttir, B., Stock, J. M., Tarasewicz, J., Martens, H. R., and Pugh, D.: Seismic imaging of the shallow crust beneath the Krafla central volcano, NE Iceland, Journal of Geophysical Research: Solid Earth, 120, 7156–7173, 2015.

Silano, G., Sreenivasan, K., and Verzicco, R.: Numerical simulations of Rayleigh-Bénard convection for Prandtl numbers between $10^{-1}$ and $10^4$ and Rayleigh numbers between $10^5$ and $10^9$, J. Fluid Mechanics, 662, https://doi.org/10.1017/S0022112010003290, 2010.

Simakin, A. and Bindeman, I.: Convective Melting and Water Behavior around Magmatic Hydrothermal Transition: Numerical Modeling with Application to Krafla Volcano, Iceland, J. Petrology, 63, egac074, 2022.

Stevens, R. J., van der Poel, E. P., Grossmann, S., and Lohse, D.: The unifying theory of scaling in thermal convection: the updated prefactors, Journal of fluid mechanics, 730, 295–308, 2013.

Teplow, W., Marsh, B., Hulen, J., Spielman, P., Kaleikini, M., Fitch, D., and Rickard, W.: Dacite melt at the Puna geothermal venture wellfield, Big Island of Hawaii, in: AGU Fall Meeting Abstracts, vol. 2008, pp. V23A–2129, 2008.

Tryggvason, E.: Widening of the Krafla fissure swarm during the 1975–1981 volcano-tectonic episode, Bulletin volcanologique, 47, 47–69, 1984.

Wadsworth, F. B., Vasseur, J., Lavallée, Y., Hess, K.-U., Kendrick, J. E., Castro, J. M., Weidendorfer, D., Rooyakkers, S. M., Foster, A., Jackson, L. E., et al.: The rheology of rhyolite magma from the IDDP-1 borehole and Hrafntinnuhryggur (Krafla, Iceland) with implications for geothermal drilling, Journal of Volcanology and Geothermal Research, 455, 108 159, 2024.

https://doi.org/10.5194/egusphere-2025-3036
Preprint. Discussion started: 7 July 2025


Witcher, T., Burchardt, S., Mattsson, T., Heap, M. J., Pluymakers, A., Li, K., and Lazor, P.: Development of permeable networks by viscous-brittle deformation in a shallow rhyolite intrusion. Part 2, 2025.

Wong, Y.-Q. and Keller, T.: A unified numerical model for two-phase porous, mush and suspension flow dynamics in magmatic systems, Geophysical Journal International, 233, 769–795, 2023.

Zierenberg, R. A., Schiffman, P., Barfod, G. H., Lesher, C. E., Marks, N. E., Lowenstern, J. B., Mortensen, A. K., et al.: Composition and origin of rhyolite melt intersected by drilling in the Krafla geothermal field, Iceland, Contributions to Mineralogy and Petrology, 165, 327–347, https://doi.org/10.1007/s00410-012-0811-z, 2013.

## Appendix A: Magma rheology

Here we provide more detail on the magma rheology, following Giordano et al. (2008); Costa et al. (2009). The viscosity of the melt phase is calculated based on the Vogel–Fulcher–Tammann (VFT) equation (Giordano et al., 2008):

$$\log \mu_m = A_i + \frac{E_i}{T - C_i}, \tag{A1}$$

where for basaltic magma $A_b$= -9.6, $E_b$ = 1.33e4, $C_b$= 307.8 K, and for rhyolitic magma $A_r$= -8.15, $E_r$ = 2.40e4, $C_r$= -431 K. These parameters are calculated for the typical melt compositions reported in Borisova et al. (2023).

Costa et al. (2009) proposed a model for the relative viscosity of the magma that depends on the second invariant of the strain-rate tensor $\epsilon$, and on the crystal content $\phi = 1 - M$, where $M$ is the melt fraction:

$$\begin{aligned}
&\eta(\phi,\epsilon) = \tfrac{1+\phi^{\delta}}{[1-F(\varphi,\epsilon,\gamma)]^{B\phi_*}} \\
&F = (1-\xi)\cdot \mathrm{erf}\left[\tfrac{\sqrt{\pi}}{2\cdot(1-\xi)}\varphi\cdot(1+\varphi^{\gamma})\right] \quad \text{with } \varphi = \tfrac{\phi}{\phi_*}, \phi = 1-M, \\
&\phi_* = 0.066499\tanh(0.913424\log(\epsilon)+3.850623)+0.591806, \\
&\delta = -6.301095\tanh(0.818496\log(\epsilon)+2.86)+7.462405, \\
&\alpha = 1-\xi = -0.000378\tanh(1.148101\log(\epsilon)+3.92)+0.999572, \\
&\gamma = 3.987815\tanh(0.8908\log(\epsilon)+3.24)+5.099645.
\end{aligned} \tag{A2}$$

In the models, one can set a scaling factor (set to 1, 10 or 100 according to test cases) as well as minimum and maximum viscosity bounds; see the values assigned to each model case in table 3.

## Appendix B: Numerical tests for mesh resolution and viscosity ranges

### B1 Mesh resolution tests

We detail here the influence of mesh resolution on the evolution of the rhyolite melting zone thickness (MZT) over time (Fig. 6). We see that for the rhyolitic intrusion (Fig.6.a), the MZT curves reach similar heights when the cell size becomes smaller than 1 m from 200 yrs onward, confirming that the maximum MZT likely to be attained is 75 m. However, after 35 years,

https://doi.org/10.5194/egusphere-2025-3036
Preprint. Discussion started: 7 July 2025


one should rather rely on the highest resolution test (resolution 0.5 m) with a value of the MZT reaching ca. 24 meters thick, whereas the 1 m resolution test reaches only ca. 16 m (30% difference).

For the basaltic intrusion (Fig.6.b), we see that a resolution of 25 cm still shows an increase by about 5 meters of the MZT with respect to the cases with resolutions between 0.4-0.5 m, which corresponds to a 20% difference. Models with a resolution ratio of 0.2 m crashed at about 15 years hence we can only observe that at that time the MZT is 3% higher than with the cases at resolution 25 cm, hence indicating that the MZT still does not converge. However let us note that these differences decrease with increasing resolution, and we can attempt to extrapolate these results: cases B.25 (cell size 25 cm) indicate that the MZT could attain 40 m about 30 years after intrusion emplacement. If the mesh size could be further increased and by visual comparison, we can reasonably add another 10-20%, so that the melt front thickness could reach $50 \pm 10$ m at time 35 years.

Following the curve shape of the rhyolite case the slope of which decreases and flattens from ca. 250 years onward, and considering that mean velocities start decreasing after 20 years in all basalt test cases, we can also evaluate that the MZT will less than double its thickness within another tens of years and until the whole system cools down back to a conductive state.

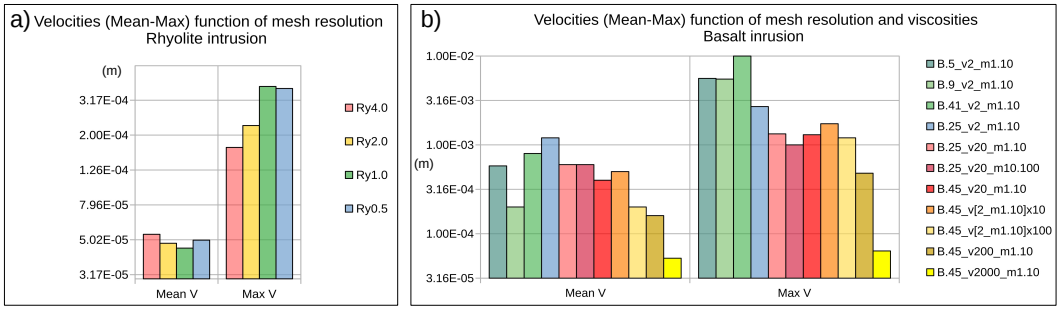


**Figure B1.** Mean and maximum velocities for model cases (ordinates in exponential scale of m/s). a) rhyolite intrusion, for 4 different mesh resolutions. b) basalt intrusion, for different mesh resolutions and different extrema viscosities (greenish for minimum viscosity $2m^2/s$, pink-red for $10m^2/s$, yellowish for greater minimum viscosities). The highest resolution cases (cell size $< 0.25$ m) are not displayed because they could not exceed 15 years and hence may not have achieved their maximum velocities.

Figs. B1 display the velocity magnitudes for each test case. For the rhyolite intrusion, we note that mean velocities remain quite similar independently of the mesh resolution. The maximum velocities increase with mesh resolution but reach a similar value for the 2 highest resolution cases, indicating mesh convergence.

Overall, these mean and maximum velocities decrease with increasing the minimum viscosity. They remain little sensitive to the mesh size once it is smaller than 1 m.

For the basalt intrusion, we display below for comparison with the case displayed Figure 7 at highest resolution, a model case with a smaller cell size of 0.45, B2. This case reached 30 years while the previous one reached only 25 years.

https://doi.org/10.5194/egusphere-2025-3036
Preprint. Discussion started: 7 July 2025


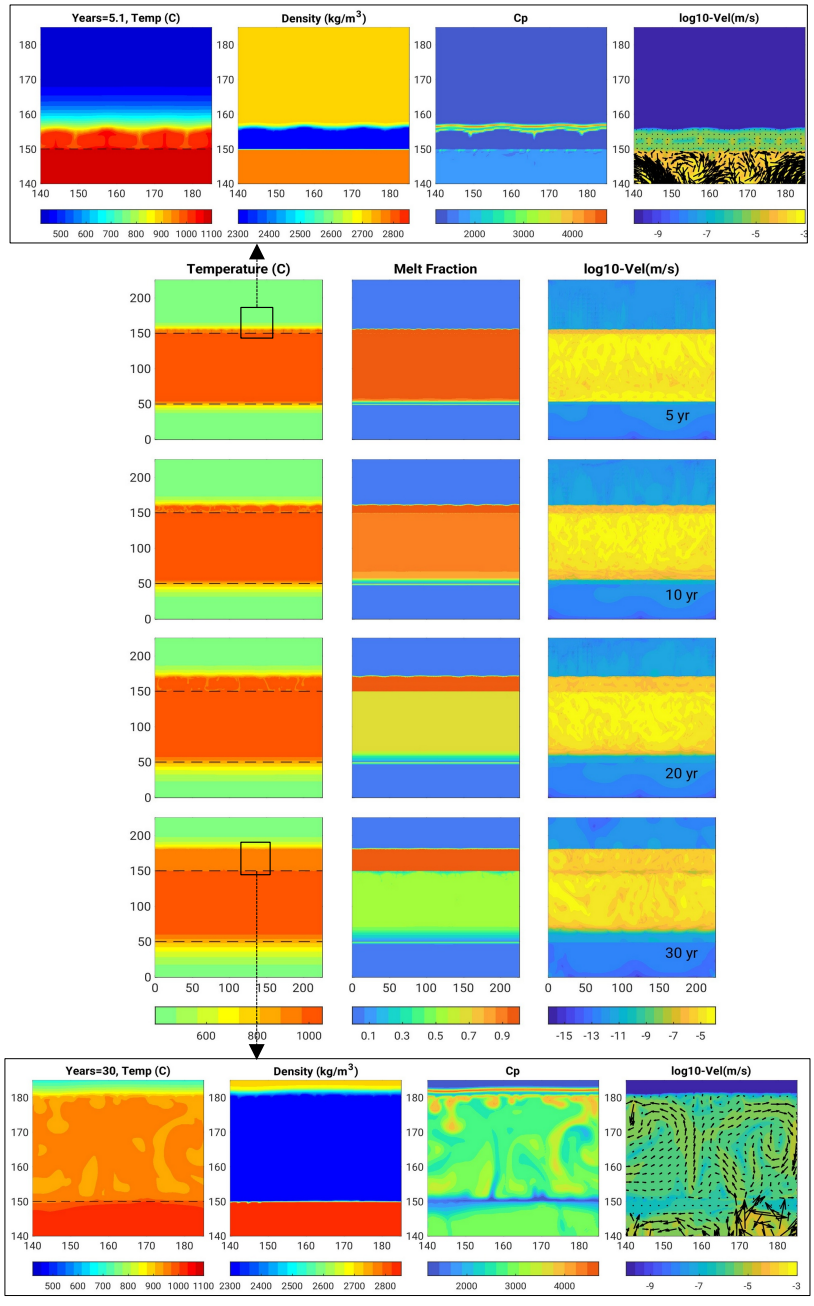


**Figure B2.** Basalt intrusion scenario (2) with greater mesh cell size 0.45 m (model B.45_v2_m5-50) than the case displayed in Figure 7 with cell size 0.25, for comparison: behavior is similar. Similar legend except that zoom snapshots are after 5 years and 30 years here.

https://doi.org/10.5194/egusphere-2025-3036
Preprint. Discussion started: 7 July 2025


## B2 Testing viscosity ranges

For the basaltic intrusion we also tested the influence of the minimum and maximum viscosities, and the values chosen in this study result from various preliminary tests. The lower limit was not varied since it is already a realistic value obtained from the melting laws given in Appendix A. The upper limit was tested: the higher this value the greater the viscosity contrast but infinite values do not make sense given the time-scale of the modelled physical process (decades). Choosing a lower viscosity for the cold bedrock must still be realistic or else it can destabilize gravitationally, as illustrated Fig. B4.

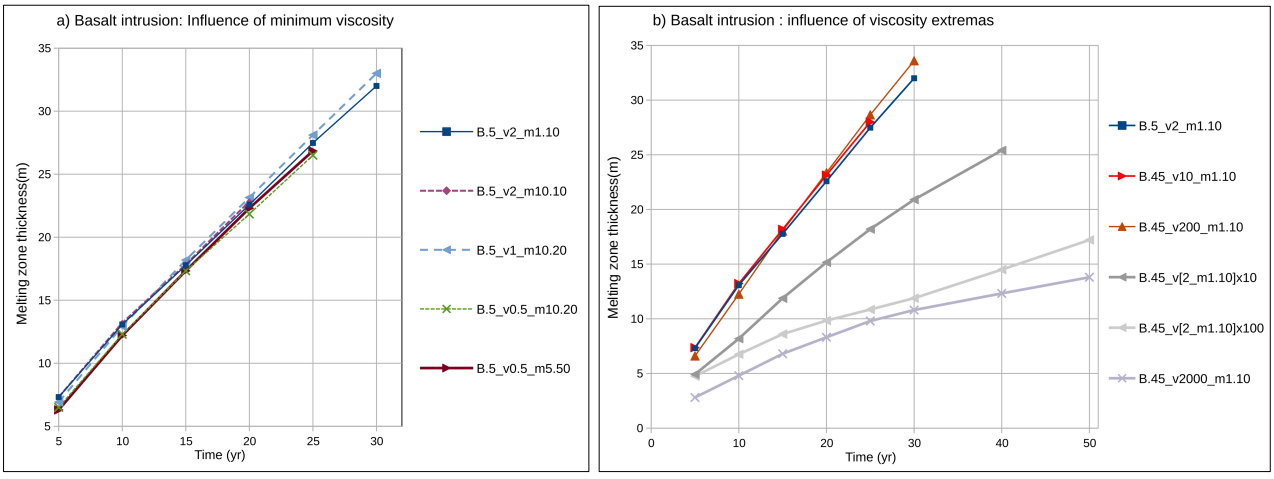


**Figure B3.** Influence of (kinematic) viscosity on the evolution of the molten rhyolite thickness for the basaltic intrusion (scenario 2). a) tests of the minimum viscosity of basalt from 0.5 to 2 $m^2/s$ and maximums ($1 - 50.10^{10}$ $m^2/s$), showing that within that range the results are very similar. b) tests of minimum viscosities from 2 to $10^3$ $m^2/s$ and maximum viscosities from $10^{10}$ to $10^{13}$ $m^2/s$. These tests have relatively low mesh resolution but at least most of them ran until 30 years.

The resulting melting zone thickness from our tests are plotted in Figures B3:

- Modifying the maximum kinematic viscosities of the rhyolite and basalt phases within a range of magnitudes does not significantly impact the results as long as they are greater than ca. $10^{10} m^2/s$. At smaller maximum values of viscosities, the entire rock mass destabilizes gravitationally and buoyant diapirs of crystallizing basalt develop into low viscosity partially melting rhyolite (cf. Fig. B4).

- Testing lower minimum viscosities for basalt was a challenge since some runs manage to go through and many more do not. The listed test cases are those that went through, indicating that a minimum basalt viscosity in the range of $0.5 - 10 m^2/s$ produces similar melting front behaviour.

- Greater overall kinematic viscosity values (multiplied by 100 or 1000 $m^2/s$) significantly impact the system's velocities and dynamics, slowing down the melting front propagation rate.

https://doi.org/10.5194/egusphere-2025-3036
Preprint. Discussion started: 7 July 2025


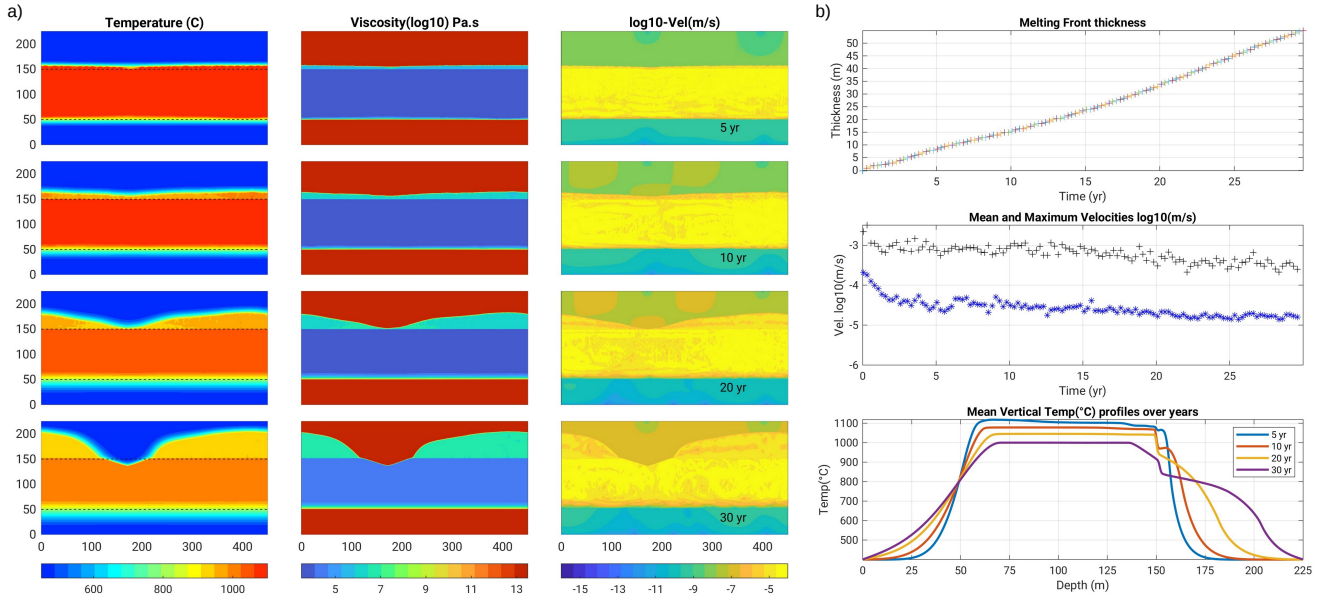


**Figure B4.** Case with a 100 m thick basalt intrusion and a weak host rock (maximum kinematic viscosity reduced to $5 \cdot 10^9 m^2/s$, model B0.5_v2_m0.5-0.5): the latter destabilizes within ca. 15 years, producing diapirism of the partially molten host rock and smoothing out of the thermal gradient. This result fits even less the sharp thermal jump observed during the IDDP-1 drilling. This case would have represented a mechanically weakened host rock due to hydrothermal fluids "mixing" with the partially molten host rock, a hypothesis that tends to be ruled out also by petrological information (see Discussion section).

## Appendix C: Thinner basalt intrusion tests

Several tests with a thinner basalt intrusion were conducted; we display here 1) a 20 m thick intrusion displaying conductive cooling after only 7 years, 2) a 50 m thick intrusion developing a 15 m thick molten rhyolite layer still convecting after 30 years.

https://doi.org/10.5194/egusphere-2025-3036
Preprint. Discussion started: 7 July 2025


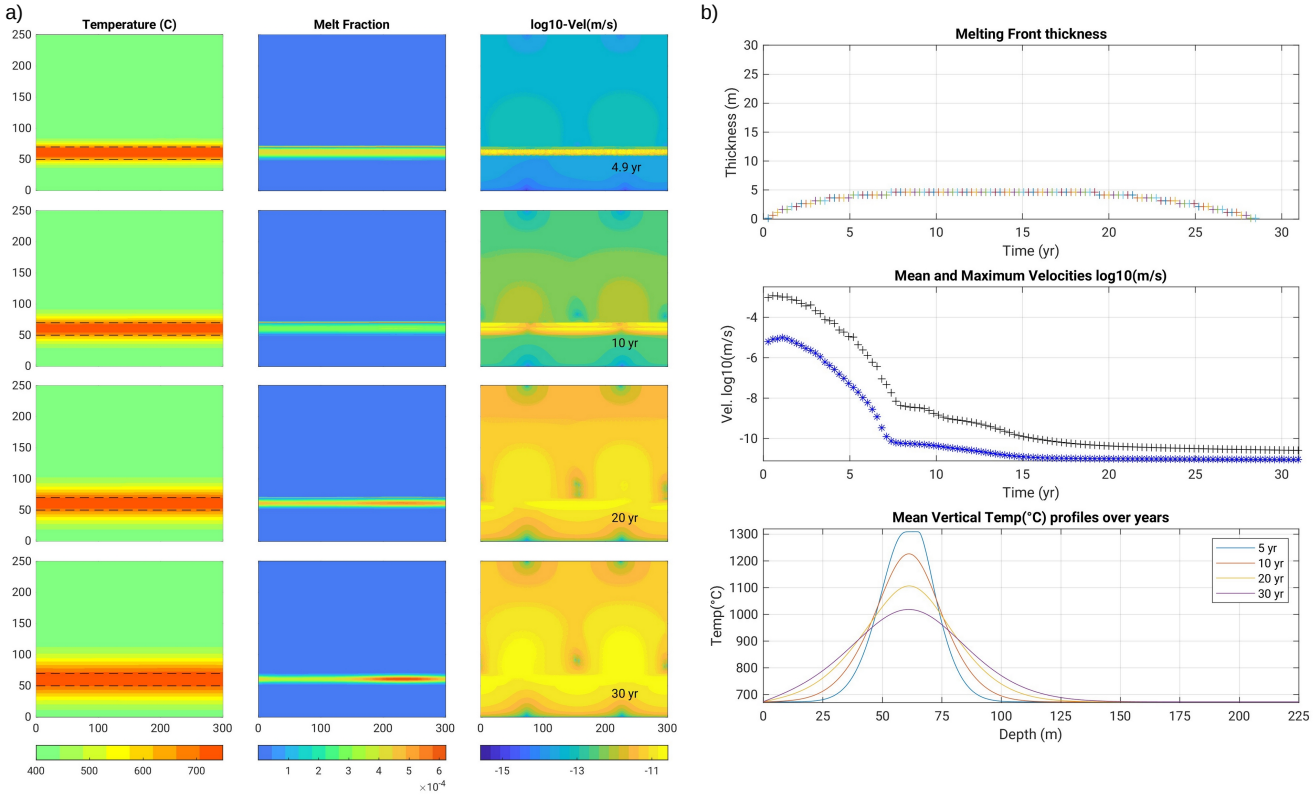


**Figure C1.** Model with a 20 m thick basalt intrusion (BT20.5_v1_m1-20). a) 4 snapshots of the temperature, melt fraction and velocity fields. Colour bar ticks are for the last displayed time step (30yrs). b) Melting front thickness and velocity magnitudes over time, and temperature profiles over depth: they become conductive after ∼7 years (velocity low and smooth temperature profile).

https://doi.org/10.5194/egusphere-2025-3036
Preprint. Discussion started: 7 July 2025


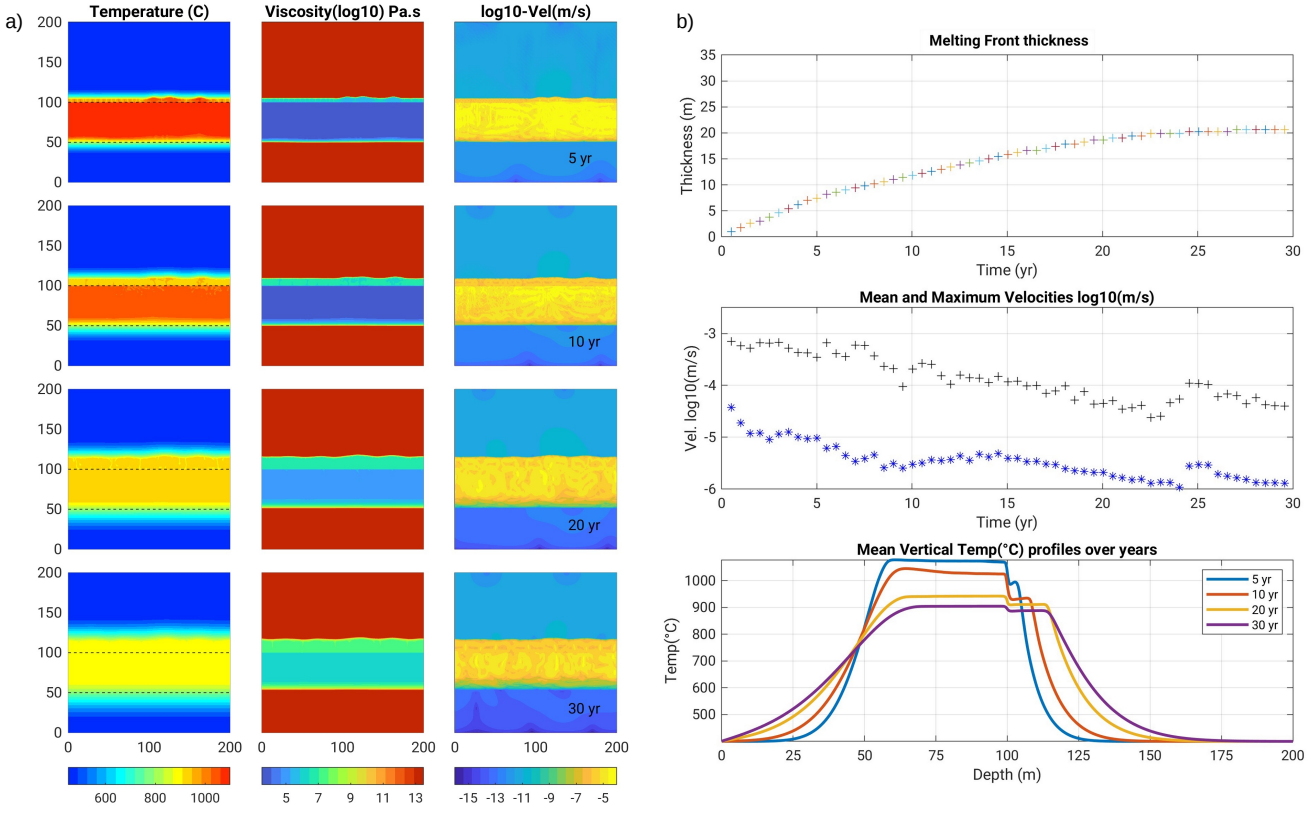


**Figure C2.** 50 m thick initial basalt intrusion (model BT50.4_v2_m5-100), for which secondary convection still occurs after 30 years, but only over ca. 20 meters. Legend same as previous figure. The 400 $^{o}$C thermal jump after 30 years now occurs over ca. 25 m, corresponding to 16$^{o}$C/m. Hence a 50 m thick intrusion may be just sufficient to explain the observed thermal gradient during the IDDP-1 drilling.